METALS AND MATERIALS, Vol. 6, No. 2 (2000), pp. 145~149

Analysis of Microstructure and Corrosion Behavior of Laser Surface Alloyed Zircaloy-4 with Niobium

Sung-Joon Lee, Hyuk-Sang Kwon and Joung-Soo Kim*

Department of Materials Science and Engineering
Korea Advanced Institute of Science and Technology
373-1 Kusong-dong, Yusong-ku, Taejon 305-701, Korea
*Steam Generator Materials Laboratory, Korea Atomic Energy Research Institute
P.O. Box 105, Yusong-ku, Taejon 305-600, Korea

The influence of laser surface alloying (LSA) with niobium (Nb) on the corrosion and mechanical properties of Zircaloy-4 was examined by potentiodynamic polarization testing in a chloride solution at 80°C and microhardness testing. The results are discussed with the structural and compositional variations in the LSA layer determined by X-ray diffraction (XRD), a scanning electron microscope (SEM) and a wavelength dispersive spectrometer (WDS). The LSA on Zircaloy-4 precoated with Nb produced a Nb-alloyed layer 200~300 μm thick with 1.3~2.5 wt.% Nb, depending on the laser beam power. The alloyed layer was composed of a mixed structure of α-Zr and β-Zr phases with the β-Zr phase increasing with the Nb content in the alloyed layer. The LSA with Nb increased the microhardness of Zircaloy-4, which was attributed primarily to the grain-size refinement of rapid cooling and, also, to the solid solution hardening with Nb. The resistance to the localized corrosion of Zircaloy-4 in a chloride solution significantly improved through LSA with Nb, which was attributed to the combined effects of the fine rapidly cooled microstructure and to the Nb alloying.

Key words : Zircaloy-4, laser surface alloying, niobium, corrosion resistance, microhardness

1. INTRODUCTION

Zirconium alloys have been extensively used as a cladding material for fuel rods in nuclear reactors, due to their low thermal neutron absorption cross-section, excellent corrosion resistance and good mechanical properties at high temperatures. Zircaloy-4 is a specific zirconium-based alloy containing, on a weight percent basis, 1.2% to 1.7% Sn, 0.18% to 0.24% Fe and 0.07% to 0.13% Cr, and was developed for use in pressurized water reactors (PWR). Zircaloy-4 tubes, however, have often been re-ported to fail by fretting corrosion occurring at the tube-grid contact due to flow-induced assembly vibration and also to erosion (debris-induced fretting) caused by such debris as Fe_3O_4 and Fe_2O_3 flowing and moving in the coolant [1,2]. Since these corrosion failures result in a reduction in the life span of the fuel cladding tube as well as in the contamination of the radioactive materials, it is necessary to improve the wear and corrosion resistance of the fuel cladding.

Alloy developments and surface treatments have been attempted to improve the corrosion and mechanical properties of Zircaloy tube. To develop a new fuel cladding alloy, intermediate alloys between the Zircaloys and Zr-Nb binaries have been actively pursued; E635 (Zr-1.2Sn-1Nb-0.4Fe) in the former USSR and ZIRLO (Zr-1Sn-1Nb-0.1Fe) by Westinghouse were developed [3,4,5]. These alloys were reported to be much less sensitive to high temperature water containing highly dissolved O_2 as well as high Li concentration. Ion implantation [6,7,8] and laser treatment [9] have been applied to modify the surface properties of the Zircaloy tube. The laser surface treatment of metals is a process where a small surface volume of materials is melted instantly by a laser beam and rapidly cooled, thereby producing very a fine microstructure with improved wear and corrosion resistance. Laser surface melting (LSM) was reported to improve the corrosion resistance of Zircaloy-4 in acid solution [9]. However, the influence of LSA with Nb or Cr on the corrosion and mechanical properties of Zircaloy-4 has not yet been studied. The objective of the present study is to form an alloyed layer with a Zr-Nb-Sn-Fe-Cr system (analogous to ZIRLO and E635) on a surface of Zircaloy-4 with the LSM technique and to examine the corrosion and mechanical properties of the alloyed layer.

2. EXPERIMENTAL PROCEDURES

The Zircaloy-4 used in this study was received in the form

Table 1. Chemical compositions (wt.%) of Zircaloy-4 used

Sn	Fe	Cr	O	Zr
1.31~1.33	0.21	0.11	0.122	bal.

of annealed sheets 1.7 mm thick. Its chemical composition is presented in Table 1. Samples with the dimensions of 35 mm×80 mm were cut from the sheets and mechanically polished down to 600 grit SiC paper, then chemically polished in 250 ml H_2O, 20 ml 70% HNO_3 and 2-3 ml 48% HF at 20°C for 5 min. To add an alloying element to the surface layer, Nb was pre-deposited on the polished sample with the DC magnetron sputtering of the Nb target in an argon atmosphere. The thickness of the precoated layer of Nb was controlled at 10 μm to produce an alloyed layer with the same Nb content as that of the Zr-2.5 wt.% Nb alloy used in CANDU reactors. We assumed that the LSM would generate a molten pool about 400 μm thick based on a previous study [10], and that the uniform mixing of the molten pool with the Nb layer occurs during the LSM. Laser processing was conducted using a continuous wave CO_2 laser at a scanning rate of 1 m/min with a beam power of 2.2 kW and 2.5 kW, respectively. The size of the final beam at the focal point was 2 mm×2 mm.

The microstructure of the laser surface alloyed samples was observed with a polarized optical microscope and a scanning electron microscope (SEM) after swab etching with 20 ml glycerol, 20 ml 70% HNO_3 and 2~3 ml 48% HF solutions. To enhance the polarization, a galvanostatic (with about 200 mA/cm^2 for a few seconds) anodization film was employed. The variation in the chemical composition of the depth of the laser surface alloyed layer was measured with a wave dispersive spectrometer (WDS)-equipped SEM. The structural ch- ange in the sample was examined by X-ray diffraction spectrometer (XRD) equipped with a copper target. The hardness of the laser alloyed surface layer was characterized by microindentation. Microhardness depth profiles were obtained from cross-sections of metallographically-prepared samples using a Vickers indenter with 200 g loads.

The effects of the LSA with Nb on the corrosion resistance of Zircaloy-4 were examined by measuring the pitting potentials that were determined from potentiodynamic polarization curves for the laser surface alloyed samples. The electrochemical cell for anodic polarization consisted of a 1 L multineck flask, with platinum counter and saturated calomel reference electrodes positioned in a salt bridge. Anodic polarization tests were performed at a sc-anning rate of 0.5 mV/s in deaerated 4 M NaCl at 80°C. The solution was deaerated by purging with high-purity nitrogen throughout the tests, starting from 1 h before the tests.

3. RESULTS AND DISCUSSION

3.1. Microstructure of laser surface alloyed Zircaloy-4

Fig. 1(a) shows the cross-sectional microstructure of the Nb-deposited Zircaloy-4 observed under polarized lighting conditions. The Nb-deposited layer grew in a columnar structure with a thickness of about 10 μm. A laser beam was irradiated on the pre-Nb-deposited samples at beam powers of 2.2 kW and 2.5 kW, and the resultant microstructures were presented respectively in Figs. 1(b) and (c). An alloyed region near the surface and an interior unalloyed region were identified in the microstructure of the laser-treated sample, which was confirmed by WDS. The thickness of the alloyed layer increased from about 170 to 270 mm with increasing beam power. The microstructure of the layer alloyed at a beam power of 2.2 kW became finer than that alloyed at 2.5 kW due to the higher cooling rate at lower beam power. A lower

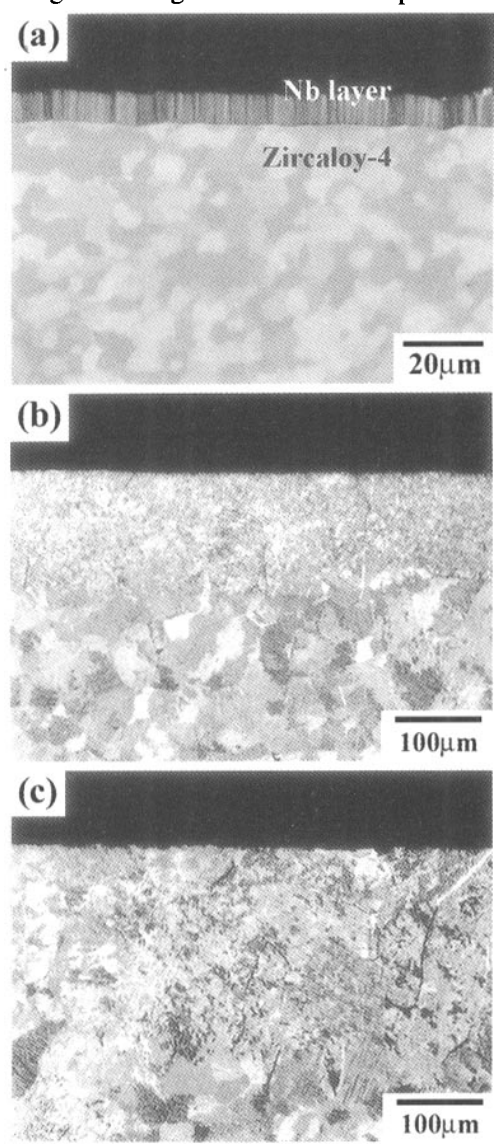

Fig. 1. Optical micrographs showing cross-sections of (a) Nb-coated Zircaloy-4, (b) laser surface Nb-alloyed Zircaloy-4 at 2.2 kW with a scan rate if 1 m/min and (c) laser surface Nb-alloyed Zircaloy-4 at 2.5 kW with a scan rate of 1 m/min.

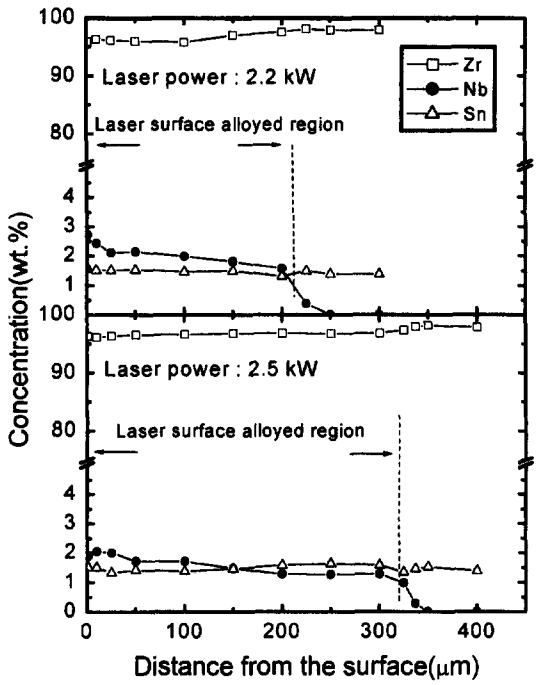

Fig. 2. Concentration profiles measured near the surface and in the sample thickness direction of laser surface alloyed Zircaloy-4 with Nb.

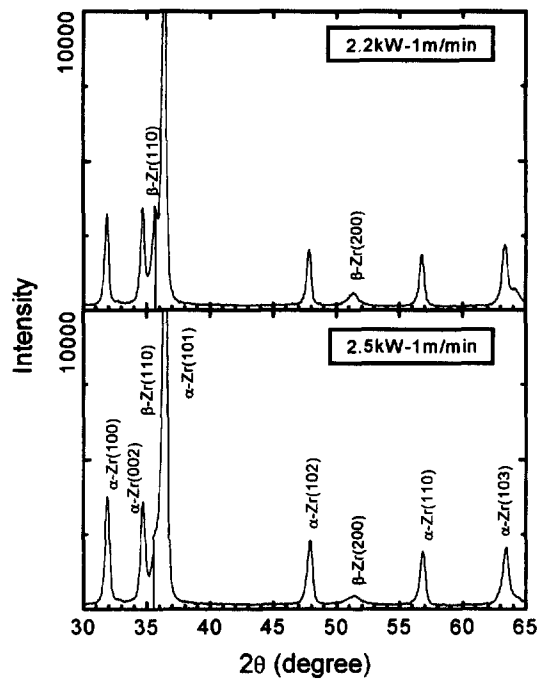

Fig. 3. XRD patterns (θ-2θ scan) of laser-treated Zircaloy-4.

beam power produces a shallower molten pool. A decrease in the molten pool volume enhances the heat sink ability via the underlying matrix, increasing the cooling rate.

Fig. 2 shows the chemical compositions with depth from the surface of the sample alloyed at different beam powers i.e., 2.2 and 2.5 kW, which were measured by WDS. With an increase in the laser beam power from 2.2 to 2.5 kW, the thickness of the alloyed layer increased about from 200 to 300 μm, which is similar to the observation from Fig. 1, while the average Nb content in the alloyed layer decreas-ed. For the sample alloyed at 2.2 kW (Fig. 2(a)), the Nb content of the alloyed layer being more than 2 wt.% at a 25 μm depth from the surface gradually decreased to 1.57 wt.% to a depth of 200 μm. The sample alloyed at 2.5 kW showed a Nb content depth profile of about 1.7 wt.% at 100 μm depth from the surface, and decreasing to 1.3 wt.% at a further depth of 200 μm. The decrease in Nb content with the increase in laser power can be attributed to the deeper and greater molten pool formed at higher laser power for a pre-deposited Nb layer with the same thickness. The Nb content in the alloyed layer did not reach the design level of an average of 2.5 wt.%, which is the result of the loss of the alloying element due to the vaporization of the Nb deposited during the laser beam melting.

The XRD patterns of the alloyed Zircaloy-4 revealed that the β-phase of the zirconium was newly formed in the alloyed layer (Fig. 3), whereas only an α-Zr phase (hcp) exists in as-received Zircaloy-4. The structure of the β-Zr phase is bcc, containing about 18.5 wt.% Nb [11]. The addition of Nb to Zr will contribute to the formation of the β-Zr phase since the Nb is a β-stabilizer. The intensity of the β-Zr peak increased when laser beam power decreased, which was the result of the increased Nb content of the alloyed layer.

3.2. Microhardness of laser surface alloyed Zircaloy-4

Microhardness depth profile of the cross-section of the laser beam-treated alloy is shown in Fig. 4. The LSA with Nb significantly increased the hardness of the Zircaloy-4 from 160 Hv for the as-received to more than 200 Hv for the laser surface alloyed sample. In particular, the hardness of the alloyed layer increased to values more than 500 Hv to the depth of 150 μm from the surface. The increase in the hardness of Zircaloy-4 with LSA can be attributed to these two effects of LSA: the alloying with Nb and the grain size refinement due to rapid cooling. The increase in hardness (ΔHv) vs. the Nb content plots suggests that of the two effects the grain size refinement is the more dominant factor in increasing the hardness of the laser surface alloyed Zircaloy-4 (Fig. 5). The slope of the ΔHv vs. the Nb content plots increased with a decrease in the beam power from 185 for the sample alloyed at 2.5 kW to 324 for the one alloyed at 2.2 kW though the values became scattered. Since the lower beam power generated a finer microstructure due to the higher cooling rate as shown in Fig. 1, the hardness of the sample alloyed with Nb at 2.2 kW was higher than that at 2.5 kW when both samples have the same Nb content. The increase in microhardness due to the LSA is expected to improve the wear resistance of Zircaloy-4, and, hence, increase the lifetime of fuel cladding tube.

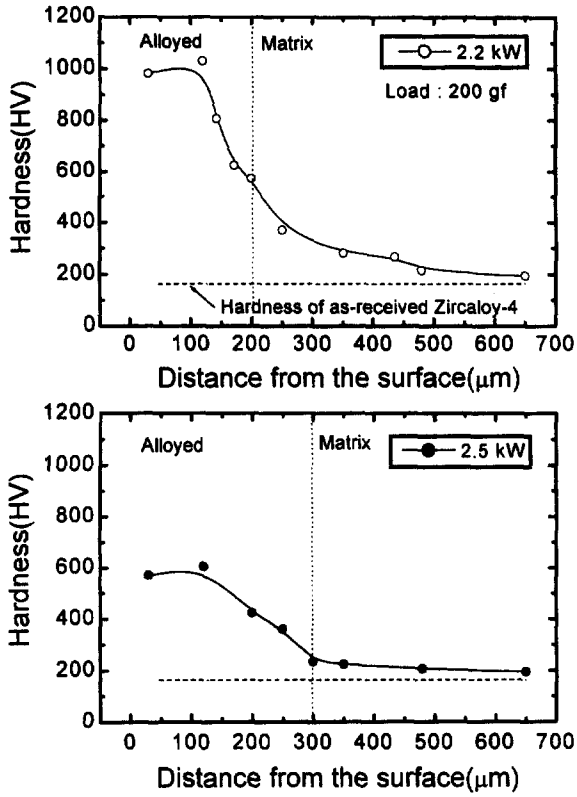

Fig. 4. Microhardnesses measured on cross-sections of laser surface alloyed Zircaloy-4 with Nb.

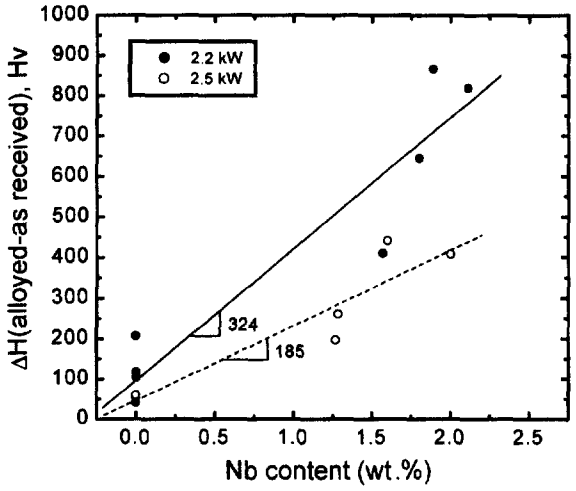

Fig. 5. Hardness variation in the Nb content in laser surface alloyed Zircaloy-4 with Nb.

3.3. Corrosion behavior of laser surface alloyed Zircaloy-4 in a chloride solution

Fig. 6 shows the effect of Nb alloying on the anodic response of Zircaloy-4 in deaerated 4 M NaCl solution at 80 °C. The resistance to the localized corrosion of the laser surface alloyed layer was enhanced as indicated by the increase

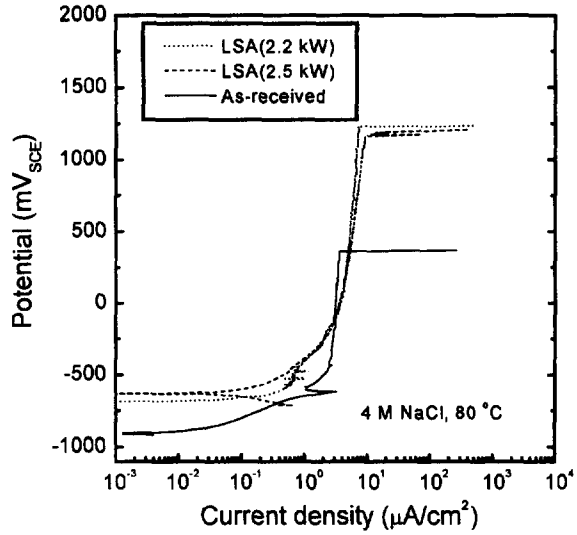

Fig. 6. Anodic polarization curves of as-received and laser surface alloyed Zircaloy-4 with Nb in deaerated 4 M NaCl at 80°C.

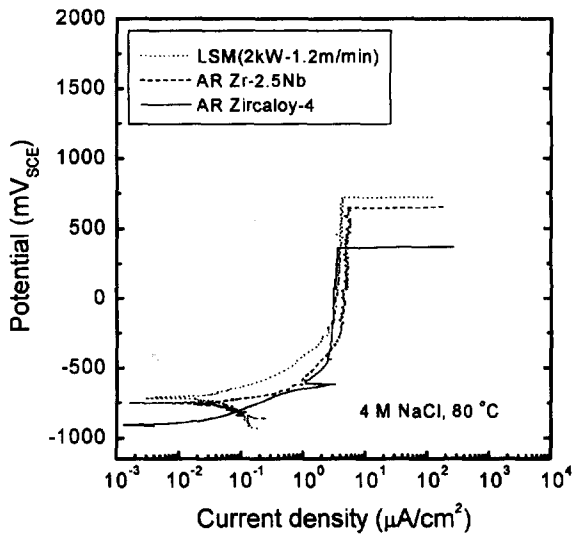

Fig. 7. Anodic polarization curves of laser surface melted Zircaloy-4 and Zr-2.5Nb in deaerated 4 M NaCl at 80°C.

in the pitting potential from 350 mV for the as-received sample to about 1200 mV for the laser alloyed sample despite the laser beams power. The influence of laser beam power on corrosion resistance was not clear unlike its influence on hardness. A further study of this is needed. Since LSA brings about two distinct effects, i.e., a fine microstructure due to rapid cooling and alloying with Nb, the respective effect of the LSA on the anodic polarization response of the alloys was examined. Fig. 7 shows the anodic polarization responses of a laser surface melted Zircaloy-4 without alloying, Zr-2.5% Nb alloy, and an as received Zircaloy-4 in a deaerated 4 M NaCl solution at 80°C. The Zr-2.5% Nb alloy is composed of a mixed structure of α-Zr and β-Zr. The pitting potential for each alloy exhibited significantly different values: 720 mV

for the laser surface melted Zircaloy-4 without alloying, and 650 mV for Zr-2.5% Nb alloy and 350 mV for the as received Zircaloy-4. Thus, it appears that the improvement in resistance to localized corrosion by the LSA with Nb can be attributed to the combined effects of the fine rapidly cooled microstructure and the alloying with Nb. In general, it has been known that grain boundaries are more susceptible to corrosion than crystals. The reason is that impurities concentrate in grain boundaries during metals solidification; the grain boundaries are in a high-energy state [12,13]. LSM can reduce the number of defects in the grain boundaries due to rapid cooling and consequently increase the corrosion resistance of the laser surface melted layer, although the layer has numerous grain boun-daries. Banikel *et al.* [14] explained that LSM improved the corrosion resistance of stainless steel AISI 321 and aluminum alloy AA6082 in a chloride solution by eliminating the preferred locations of pit formation such as precipitates, inclusions and other defects; small noncrystallographic shallow pits formed and uniform corrosion attack occurred on the laser surface melted layer of the aluminum alloy due to the ultra-fine microstructure of the layer.

4. CONCLUSIONS

(1) LSA on Zircaloy-4 produced a Nb-alloyed layer 200~300 μm thick woth 1.3~2.5 wt.% Nb, depending on laser beam power. With increasing laser beam power, the Nb content in the alloyed layer decreased because a deeper and greater molten pool was formed at higher laser power for a pre-deposited Nb laser of constant thickness. The alloyed layer was composed of a mixed structure of α-Zr and β-Zr phases with the β-Zr phase being increased with the Nb content in the alloyed layer.

(2) LSA increased the microhardness of Zircaloy-4, which was attributed primarily to the grain-size refinement by rapid cooling and also to the solid solution hardening with Nb.

(3) The resistance to localized corrosion of Zircaloy-4 in a chloride solution was significantly improved by LSA with Nb, which was attributed to the combined effects of the fine rapidly cooled microstructure and Nb alloying.

ACKNOWLEDGMENT

This work was done under '97 Nuclear R&D supported by The Korean Ministry of Science and Technology and '97 Electrical Technique Research supported by The Electrical Engineering & Science Research Institute.

REFERENCES

1. E. Hillner, *Proc. Zirconium in the Nuclear Industry, ASTM STP 633* (eds., A. L. Lowe, Jr. and G. W. Parry), p. 211, ASTM, Philadelphia (1977).
2. E. H. Novendstern, *Meetings on Fuel Performance*, KEPCO/KINS/Westinghouse, KAERI, Taejon (1994).
3. G. P. Sabol, G. R. Klip, M. G. Balfour and E. Roberts, *Proc. 8th Int. Symp on Zirconium in the Nuclear Industry, ASTM STP 1023* (eds., L. F. P. Van Swan and C. M. Eucken), p. 227, ASTM, Philadelphia (1989).
4. A. V. Nikulina, V. A. Markelov, M. M. Peregud, Y. K. Bibilashvili, V. A. Kotrekhov, A. F. Lositsky, N. V. Kuzmenko, Y. P. Shevnin, V. K. Shamardin, G. P. Kobylyansky, A. E. Novoselov, *Proc. 11th Int. Symp on Zirconium in the Nuclear Industry, ASTM STP 1295* (eds., E. R. Bradley and G. P. Sabol), p. 785, ASTM, Philadelphia (1996).
5. R. J. Comstock, G. Schoenberger and G. P. Sabol, *Proc. 11th Int. Symp on Zirconium in the Nuclear Industry, ASTM-STP 1295* (eds., E. R. Bradley and G. P. Sabol), p. 711, ASTM, Philadelphia (1996).
6. W. Kim, K. S. Jung, B. H. Choi, H. S. Kwon, S. J. Lee, J. G. Han and M. I. Guseva, *Surf. Coat. Tech.* **76-77**, 595 (1995).
7. G. Tang, B. H. Choi, W. Kim, K. S. Jung, H. S. Kwon, S. J. Lee, J. H. Lee, T. Y. Song, D. H. Shon and J. G. Han, *Surf. Coat. Tech.* **89**, 252 (1997).
8. S. J. Lee, H. S. Kwon, W. Kim and B. H. Choi, *Mater. Sci. Eng. A* **263**, 23 (1999).
9. W. Reitz and J. Rawers, *J. Mater. Sci.* **27**, 2437 (1992).
10. H. S. Kwon and S. J. Lee, *A Study on the Improvement of Corrosion Resistance of Fuel Cladding Material by Surface Modification*, p. 64, EESRI 97-015, EESR1 (1998).
11. J. P. Abriata and J. C. Bolcich, *Bull. Alloy Phase Diagrams* **3**, 1710 (1982).
12. D. M. Follstatedt, *Laser and Electron-Beam Interactions with Solids: Proc. of the Materials Research Society Annual Meeting* (eds., B. R. Appleton and G. K. Celler), p. 377, North Holland, New York (1982).
13. D. L. Piron, *The Electrochemistry of Corrosion*, p.164, NACE International, Houston, TX (1991).
14. J. Barnilkel, T. Seefeld, A. Emmel, E. Schubert and H. W. Bergmann, *JOM* **48**, 29 (1996).